Laser Micro-Structuring on Glass Substrates with Compensation Function for Multi-wavelength Mixed Laser Diode Module

Yi-Cheng Lin, Chih-Chung Yang, Kuo-Cheng Huang and Wen-Tse Hsiao
Instrument Technology Research Center, National Applied Research Laboratories, 20, R&D Rd. VI. Hsinchu Science Park, Hsinchu City, Taiwan

Keywords: Ultraviolet Laser System, Multi-wavelength Mixed Light Module, High-Speed Galvanometric Scanner, Surface Micro-Structures, Laser Matter Interaction, Light Compensation Effects, Chrominance.

Abstract: A glass substrate has excellent optical transmittance for the visible spectrum (400–700 nm). This study used three type glass (D263T^{TM}, EAGLE XG$^{\circ,R}$, and BK7) for laser micro-structuring in the light compensation technique applied to a multi-wavelength mixed light module. An ultraviolet laser system combined with a high-speed galvanometric scanner was used to fabricate microstructures on the specimen surface. The light compensation chromaticity properties of the microstructures on glass substrates depended on the laser machining conditions. The characteristics of the machined glass were systematically analyzed using a spectrophotometer and charge-coupled device camera. The experimental results demonstrate that the microstructures affected chromaticity under different laser micro-structuring pitches.

1 INTRODUCTION

Micro-projection technology comprises conventional projection technology, including laser scanning, digital lighting process, transmission LCD, and liquid crystal on silicon. Limited by inherent size and power loss issues, miniature projection optical systems use light-emitting diodes (LEDs) or collimated laser light sources. However, laser light sources, with their high brightness, high single-frequency, and high directivity, offer a higher contrast and improved visual experience. In the distribution of the color range, laser light sources have high color saturation, yet retain the advantages of other light sources used for projection. Micro-projection technology is expected, in the next generation, to be eventually replaced by laser light sources with improved saturation and to contribute to new products such as automobile lights.

However, laser light sources do not emit white light, but generate it by mixing three different wavelengths: red (R), green (G), and blue (B). As a result, RGB laser light comprises different wavelengths, and the intensity of its radiated energy differs for colder or warmer colours. Several sources in the literature discuss using laser sources to fabricate periodic and non-periodic structures on different materials.

(Florea, 2003) used a femtosecond laser to fabricate the lines and curves of a waveguide structure on silicate glass and a Fabry–Pérot resonator to measure the waveguide loss. In addition, a 10-μm periodic grating was annealed for different durations. The results indicate that the diffraction efficiency was approximately 8%. (Zheng, et al. 2004) and (Hee, et al. 2005) used a femtosecond laser to produce a periodic structure on fused silica and crystalline silicon materials by using an interference lithography method. (Zheng, et al. 2004) used a P-polarization femtosecond laser to fabricate a crack-free periodic grating structure with a 20-μm line width, and the vertical microstructure had significant polarization. (Hee, et al. 2005) used four types of polarization modes to fabricate a periodic microstructure. The results indicated that the polarization mode affected the grating depth, surface roughness, and removal threshold. (Florea et al., 2008), (Cho et al., 2008), and (Ams et al., 2008) used the femtosecond laser pulse properties to produce a two-dimensional structure of the interior of the glass substrate that could take advantage of the light guide according to the principle of optical glass translucent color and other optical properties. (Oliveira et al., 2009) used a range of laser pulse energy, from 0.5 J/cm^2 to 2 J/cm^2, to produce micro-, nano-, and nonperiodic titanium microstructures.

Lin Y., Yang C., Huang K. and Hsiao W.
Laser Micro-Structuring on Glass Substrates with Compensation Function for Multi-wavelength Mixed Laser Diode Module.
DOI: 10.5220/0006106601690174
In *Proceedings of the 5th International Conference on Photonics, Optics and Laser Technology (PHOTOPTICS 2017)*, pages 169-174
ISBN: 978-989-758-223-3

The results indicated that the shock wave diffused outwards from the center. In addition, scan speeds affected the periodic structure, making the laser energy lower than the ablation threshold that could generate various periodic micro- and nanostructures on titanium substrates. (Hsiao, et al. 2016) used simulation and experiment verification of pulsed ultraviolet laser micromilling technology on soda-lime and B270 glass, to discuss the effect depth and surface roughness of laser milling parameters. The experimental results indicated that the milling speed increased with an increase in the pulse repetition frequency. The milling depth increased with an increase in the number of milling passes. This study uses a UV laser source in conjunction with a galvanometric scanner to fabricate microstructures on three type glass (D263T^{TM}, EAGLE XG$^{\bigcirc,R}$, and BK7) for laser micro-structuring in the light compensation technique applied to a multi-wavelength mixed light module..

2 LASER MICROMACHINING SYSTEM AND PREPARED SAMPLE

2.1 UV Laser Micro-milling System and Sample Prepared for Micro-structuring Fabrication

A diode-pumped solid-state (DPSS) Nd:YVO4 UV laser (wavelength 355 nm, maximum output power level 14 W, transverse mode TEM00, output beam diameter 3.5 mm) (COHERENT, Inc., AVIA 355-14) was combined with a high-speed galvanometer system (Raylase AG model SS-15), in which a focus shifter was used to adjust the focus range in the Z-direction from +15 to −15 mm on an x/y axis moving stage. A telecentric focusing lens with a focal length of 163 mm and a scanning area of 60 mm2 was used for micromilling, and the operation pulse repetition frequency ranged from 1 to 400 kHz. Table 1 summarizes the complete specifications of the DPSS laser milling system. Table 2 summarizes three types of substrates for the microstructure fabrication, including a double-sided polished Corning EAGLE XG $^{\bigcirc,R}$ glass and SCHOTT D263T^{TM}. The machined specimens were cleaned in an ultrasonic cleaner with a solution of 75% alcohol and 25% distilled water. The specimens were dried on a spin coater, followed by baking and curing at 50 °C for 10 minutes. The overlapping rate affected the milled edge quality, surface roughness, and removal rate. The factors influencing the overlapping rate included the scan speed of the galvanometric unit, the frequency of the pulse repetition, the diameter of the focused beam, and the bite size of each overlapped laser beam. The bite size and overlapping rate can be calculated using Equations (1) and (2) respectively:

$$B_s = \frac{V}{f} \quad (1)$$

$$O_R(\%) = \frac{b - B_s}{b} \times 100 \quad (2)$$

where B_s is the bite size (mm), V is the scan speed (mm/s), f is the pulse repetition frequency (Hz), OR is the overlapping rate, and b is the laser beam spot size (mm) as shown in Figure 1.

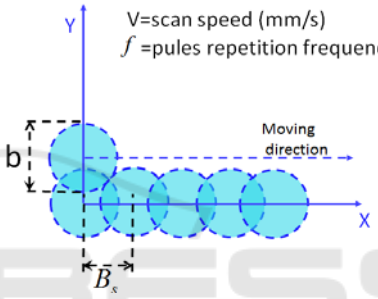

Figure 1: Schematic diagram of the laser beam overlapping rate.

Table 1: Specification of the DPSS laser milling system.

Item	Parameters
Wavelength (nm)	355
Average power (watt)	> 14
Laser mode	TEM_{00}
Pulse repetition frequency (kHz)	~ 400
Pulse width (ns)	28
Focused beam size (μm)	30
Machining field (mm^2)	60

Table 2: Three types of substrate for the microstructure fabrication.

Material	Commercial BK7	EAGLE XG$^{\bigcirc,R}$ glass	D263T^{TM} glass
Polished	DSP	DSP	DSP
Thickness	1.5 mm	0.7 mm	0.55 mm
Transmittance (400-700nm)	> 87%	> 92%	> 87%

Three types of substrate with thicknesses of 0.7 mm (EAGLE XG$^{\bigcirc,R}$) and 0.55 mm (D263T^{TM}) were used for milling. To evaluate the illumination, uniformity, and chromaticity properties, the micro-

structuring area was fixed at 30 × 30 mm [see Figure 2 (a)]. Figure 2 (b) shows the schematic of the planned laser milling path. Each milling area (30 × 30 mm) was used for evaluation at intervals of 1 μm in the horizontal and vertical directions. Moreover, the milling angle of the horizontal path was set to 0° and the vertical path was set to 90°. In addition, the laser milling speed and frequency was fixed at 2000 mm/s and 100 kHz, respectively. Table 3 shows the laser milling parameters for the milling of Corning EAGLE XG$^{\bigcirc,R}$ glass and SCHOTT D263T^{TM}.

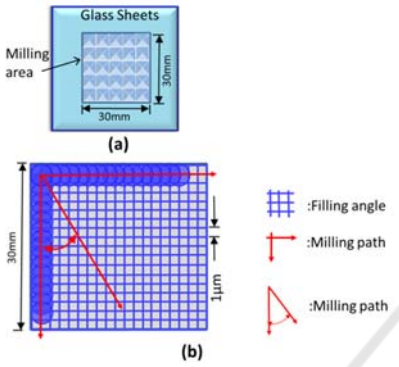

Figure 2: Experimental setup; (a) laser milling region and (b) laser milling path planning.

3 MEASUREMENT SYSTEM SETUP

Three monochromatic laser diodes providing R, G, and B lights, respectively, were mixed sequentially to assemble a mixed light measurement on the platform for controlling the single lights (R, G and B); two-color light mixing (R/G, G/B, and R/B); and three-color light mixing (R/G/B).

These were subsequently combined with the machined micro-structuring light compensation optics. In addition, to characterize the color of the samples, the transmittance spectra were measured with a spectrophotometer (OtO, SE1220). From the spectra evaluation, the standard CIE 1931 chromaticity coordinates of the different colors were calculated. The illumination, uniformity, color, and other indicators were measured before and after compensation. Figure 3 shows the schematic diagram of the measurement setup of the micro-optical elements were configured to compensate for various types of mixed light, according to the optical properties of the model, for analyse their effects.

To understand the microstructural elements with and without light compensation for the optical

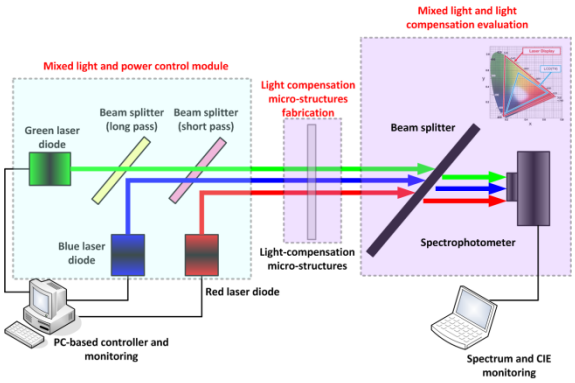

Figure 3: Schematic diagram of the mixed light module for RGB laser diode.

characteristics of each type of light-mixing mode of influence, the laser light intensity calculation system was analyzed with a laser power meter and laser beam after quality measurements were recorded of the actual instrument with microlight compensation structures for laser power and spot quality. For color uniformity and analysis, a spectrophotometer was employed. In this study, the International Commission on Illumination (CIE) 1931 standard colorimetric analysis of post-RGB mixed laser light sources, the common standard color matching functions of R/G/B wavelengths were 671 nm/532 nm / 473 nm, and the sequential color ratio of 1 : 0.098: 0.329 is defined as the standard for mixed white light.

The XYZ color space is the sum of the three colors. Its two-dimensional coordinates are calculated in Equation (3).

$$x = \frac{X}{X+Y+Z} \quad y = \frac{Y}{X+Y+Z} \quad z = \frac{Z}{X+Y+Z} \tag{3}$$

In addition, its color matching and power distribution as converted by the RGB spectrum are represented in Equation (4).

$$\begin{aligned} \mathrm{X} &= \mathrm{k} \int_{vis} P(\lambda) \cdot \bar{x}(\lambda) d\lambda \\ Y &= k \int_{vis} P(\lambda) \cdot \bar{y}(\lambda) d\lambda \\ \mathrm{Z} &= \mathrm{k} \int_{vis} P(\lambda) \cdot \bar{z}(\lambda) d\lambda \end{aligned} \tag{4}$$

where k is the normalized coefficient in Equation (5) and P (λ) is the energy distribution of the light source. In addition, the RGB, CIE, and XYZ values constitute the 3 × 3 matrix in Equation (6).

$$\mathrm{k} = \frac{100}{\int_{vis} P(\lambda) \cdot \bar{y}(\lambda) d\lambda} \tag{5}$$

$$\begin{bmatrix} R \\ G \\ B \end{bmatrix} = \begin{bmatrix} 3.240479 & -1.537150 & -0.498535 \\ -0.96925 & 1.875992 & 0.041556 \\ 0.055648 & -0.204043 & 1.057311 \end{bmatrix} * \begin{bmatrix} X \\ Y \\ Z \end{bmatrix}$$

$$\begin{bmatrix} X \\ Y \\ Z \end{bmatrix} = \begin{bmatrix} 0.412453 & 0.357580 & 0.180423 \\ 0.212671 & 0.715160 & 0.072169 \\ 0.019334 & 0.119193 & 0.950227 \end{bmatrix} * \begin{bmatrix} R \\ G \\ B \end{bmatrix} \quad (6)$$

4 RESULTS AND DISCUSSION

4.1 Without Optical Component: RGB Mixed Light Projection and CIE Chromaticity Analysis

On the basis of the measurement architecture of Figure 3, the RGB laser beams were directly projected onto a white card, after which the voltage of the lasers was adjusted and spectra of the mixed laser spots were captured by the spectrophotometer for the different chromaticities of light. By using charge-coupled device (CCD) camera to capture the image on the white paper are shown in Fig 4 (a-f).

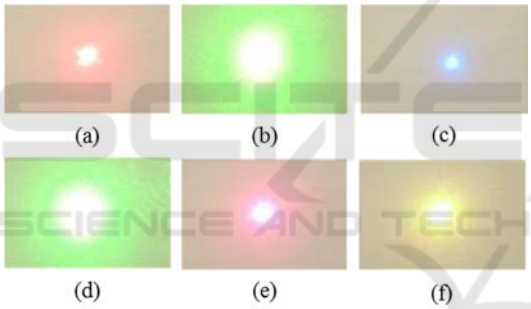

Figure 4: Projection light image on white paper without any optical compensation components (a) R light, (b) G light, (c) B light, (d) R/G mixed light, (e) G/B mixed light, and (f) R/B light captured by CCD camera.

Figure 5 (a-c) shows the CIE 1931 diagram and its x and y coordinate of single R, G, and B light without optical compensation component, respectively. The center point of green light was found to be more saturated than the others, and therefore the proportion of green light had to be decreased during colour mixing. Figure 5 (d-f) shows the spectrum and CIE 1931 diagram of the two color R/G, G/B, and R/B color mixing. Figure 5 (d) shows the green tone obtained when G and B are at full load and R is off. Figure 5 (e) shows the red tone obtained when R and B are at full load and G is off. Figure 5 (f) shows the yellow tone obtained by when R and G are at full load and B is off. However, because white light cannot be obtained through two-color mixing, the voltage of light sources must be adjusted for color mixing. Figure 5 (g) shows the R/G/B mixed light generated when the voltage of light sources is R = 0.74 voltage, G = 0.49 voltage, and B = 2.19 voltage. The x and y coordinate was 0.3051 and 0.3034, respectively.

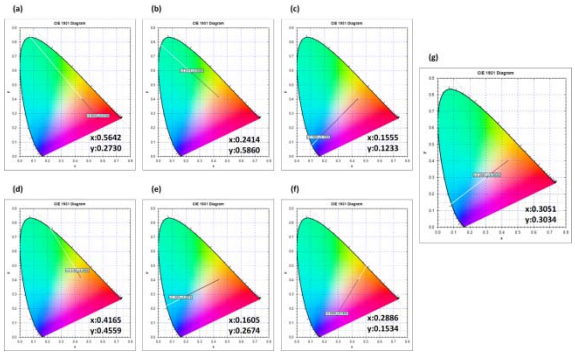

Figure 5: Results of the monochromatic light without any optical compensation components (a) R light, (b) G light, (c) B light, (d) R/G mixed light, (e) G/B mixed light, (f) R/B light, and (g) R/G/B light captured by spectrophotometer.

4.2 With Optical Component: RGB Mixed Light Projection and CIE Chromaticity Analysis

Figure 6 shows the three types (EAGLE XG$^{\bigcirc,R}$, D263T^{TM}, BK7) fabricated optical components with micro-structuring on surface fabricated by UV laser milling. As same as the monochromatic light measurement method, the optical component (with microstructure) was assembled in the mixed light module.

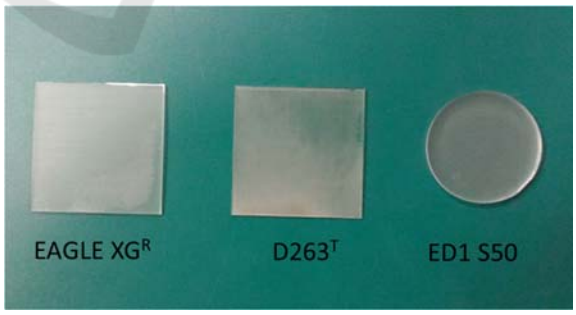

Figure 6: Images of the three type optical component with micro-structure.

Table3 to Table 5 summarized the CIE 1931 diagram evaluation results and its x and y coordinate of single R, G, and B light and mixed light of three type components (i.e. Corning EAGLE XG$^{\bigcirc,R}$ glass, D263T^{TM} and BK7 optical compensation component, respectively. Compared with the

original single monochrome light source (R, G, and B), by using three type optical components with microstructure. The CIE 1931 diagram shows the coordinate moved toward to the white light region coordinate.

Compared with the two color (R/G) mixed light source, by using three type optical components with microstructure. The CIE 1931 diagram shows the coordinate moved toward to the white light region coordinate by using EAGLE XG $^{\bigcirc,R}$ glass and D263T^{TM} glass. By using the BK7 glass, the coordinate was moved toward to yellow color spectrum. Compared with the two color (G/B) mixed light source, by using three type optical components with microstructure. The CIE 1931 diagram shows the coordinate moved toward to the white light region coordinate by using EAGLE XG$^{\bigcirc,R}$ glass and BK7 glass. By using the D263T^{TM} glass, the coordinate was moved toward to depth blue coordinate. Compared with the two color (R/B) mixed light source, by using three type optical components with microstructure. The CIE 1931 diagram shows the coordinate moved toward to the depth blue region coordinate by using D263T^{TM} glass and BK7 glass. By using the EAGLE XG$^{\bigcirc,R}$ glass, the coordinate was moved toward to white light region coordinate.

Compared with the three color (R/G/B) mixed light source, by using three type optical components with microstructure. The CIE 1931 diagram shows the coordinate moved toward to white light region coordinate by using EAGLE XG$^{\bigcirc,R}$ glass. By using the D263T^{TM} glass and BK7 glass, the coordinate was moved toward to depth blue light region coordinate. Figure 7 shows the CIE 1931 diagram of the three type optical component with microstructure. As the experimental results indicated that the EAGLE XG$^{\bigcirc,R}$ glass have the best light compensation consequent.

Table 3: Summaries the CIE 1931 diagram x and y coordinate evaluation results using Corning EAGLE XG$^{\bigcirc,R}$ glass.

Coordinate / Light source	X	Y
R light	0.4794	0.3243
G light	0.2825	0.4891
B light	0.2149	0.1990
R,G mixed light	0.4073	0.4162
G,B mixed	0.2072	0.3021
R,B mixed	0.3364	0.2186
R,G,B mixed	0.3061	0.3034

(R: red, G: green, B: blue)

Table 4: Summaries the CIE 1931 diagram x and y coordinate evaluation results using SCHOTT D263T^{TM}.

Coordinate / Light source	X	Y
R light	0.4663	0.3101
G light	0.2562	0.5068
B light	0.1796	0.1483
R,G mixed light	0.3782	0.4324
G,B mixed	0.1790	0.2492
R,B mixed	0.2591	0.1547
R,G,B mixed	0.2527	0.2462

(R: red, G: green, B: blue)

Table 5: Summaries the CIE 1931 diagram x and y coordinate evaluation results using BK7.

Coordinate / Light source	X	Y
R light	0.5434	0.3145
G light	0.2301	0.5988
B light	0.1692	0.1499
R,G mixed light	0.3903	0.4932
G,B mixed	0.1672	0.3006
R,B mixed	0.2885	0.1779
R,G,B mixed	0.2517	0.2900

(R: red, G: green, B: blue)

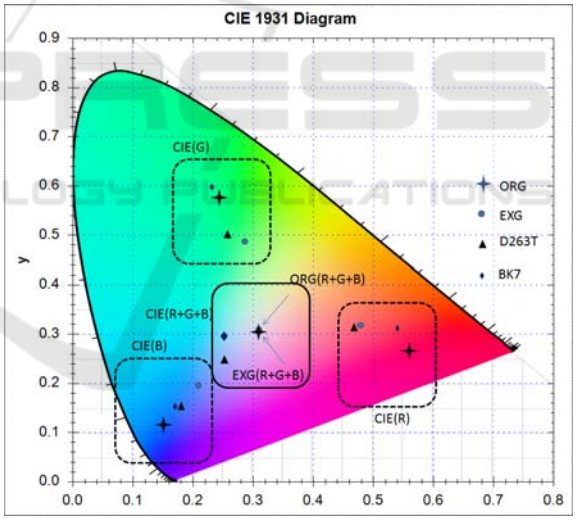

Figure 7: CIE 1931 diagram of with and without light-compensation components.

5 CONCLUSIONS

This study used an ultraviolet laser system combined with a high-speed galvanometric scanner unit to mill optical glass substrates, creating optical microstructures, and then analyse them with software to simulate the area and size of uniform light projections. By controlling the ratio of laser

light at three wavelengths and conducting CIE analysis, similar white laser light can be modulated over time. In the experimental results, the CIE 1931 diagram shows the coordinate moved toward to white light region coordinate by using EAGLE XG$^{\bigcirc,R}$ glass. By using the D263TTM glass and BK7 glass, the coordinate was moved toward to depth blue light region coordinate. As the experimental results indicated that the EAGLE XG$^{\bigcirc,R}$ glass has the best light compensation consequent. This system can modulate laser light according to user demand in fields such as medicine, microelectronics, and conventional lasers.

REFERENCES

Florea, C., Winick, K. A., 2003. Fabrication and characterization of photonic devices directly written in glass using femtosecond laser pulses. *J. Lightwave Technol.*, Vol. 21, pp. 246-253.

Zheng, H. Y., Zhou, W., Qian, H. X., Tan, T. T., Lim, G. C., 2004. Polarisation-independence of femtosecond laser machining of fused silica. *Appl. Surf. Sci.*, Vol. 236, pp. 114-119.

Hee, C. W., Ngoi, B. K. A., Lim, L. E. N., Venkatakrishnan, K., Liang, W.L., 2005. Effect of polarization on femtosecond pulsed laser ablation of surface relief gratings using a novel interferometer. *Opt. Laser Technol.*, Vol. 37, pp. 93-98.

Florea, C., Sanghera, J. S., Aggarwal, I. D., 2008. Direct-write gratings in chalcogenide bulk glasses and fibers using a femtosecond laser. *Opt. Mater.*, Vol. 30, pp. 1603-1606.

Cho, S. H., Chang, W. S., Kim, J. G., Kim, K. R., Hong, J.W., 2008. Fabrication of internal diffraction gratings in planar fluoride glass using low-density plasma formation induced by a 26 femtosecond laser, *Appl. Surf. Sci.*, Vol. 255, pp. 2069-2074.

Ams, M., Marshall, G. D., Dekker, P., Dubov, M., Mezentsev, V.K., Bennion, I., Withford, M.J., 2008. Investigation of ultrafast laser–photonic material interactions: challenges for directly written glass photonics. *IEEE J. Sel. Top. Quant.*, Vol. 14, pp. 1370-1381.

Oliveira, V., Ausset, S., Vilar, R., 2009. Surface micro/nanostructuring of titanium under stationary and non-stationary femtosecond laser irradiation. *Appl. Surf. Sci.*, Vol. 255, pp. 7556-7560.

Hung, M. W., Chen, C. J., Chang, C. L., Hsu, C. W., 2011. The impacts of high frequency pulse driving on the performance of LED light", Phys. Procedia, Vol. 19, pp. 336-343.

Billmeyer, F. W., Saltzman, J. M., 1981. Principles of Color Technology, 2nd edition, John Wiley & Sons, Inc., New York.

Zukauskas, A., Shur, M. S., Gaska, R., 2002. Introduction to Solid State Lighting, John Wiley & Sons, Inc., New York.

Hsiao, W. T., Yang, C. C., Huang, K. C., Chung, C. K., Tseng, S.F., Chiang, D., Chen, M. F., 2016. Optical glass substrates forming processes using pulsed ultraviolet laser micromilling technology, *J. Laser Micro. Nanoen.*, Vol. 11, pp. 30-34.